HAL open science

Study of GaN layer crystallization on GaAs(100) using electron cyclotron resonance or glow discharge N2 plasma sources for the nitriding process

H. Mehdi, F. Réveret, Catherine Bougerol, C. Robert-Goumet, P.E. Hoggan, L. Bideux, B. Gruzza, J. Leymarie, G. Monier

▶ **To cite this version:**

H. Mehdi, F. Réveret, Catherine Bougerol, C. Robert-Goumet, P.E. Hoggan, et al.. Study of GaN layer crystallization on GaAs(100) using electron cyclotron resonance or glow discharge N2 plasma sources for the nitriding process. Applied Surface Science, 2019, 495, pp.143586. 10.1016/j.apsusc.2019.143586 . hal-02345167

HAL Id: hal-02345167

https://hal.science/hal-02345167v1

Submitted on 20 Jul 2022

HAL is a multi-disciplinary open access archive for the deposit and dissemination of scientific research documents, whether they are published or not. The documents may come from teaching and research institutions in France or abroad, or from public or private research centers.

L'archive ouverte pluridisciplinaire **HAL**, est destinée au dépôt et à la diffusion de documents scientifiques de niveau recherche, publiés ou non, émanant des établissements d'enseignement et de recherche français ou étrangers, des laboratoires publics ou privés.

Distributed under a Creative Commons Attribution - NonCommercial 4.0 International License

Version of Record: https://www.sciencedirect.com/science/article/pii/S0169433219323839
Manuscript_7776b6c64cf34c87444367ed3784754d

Study of GaN layer crystallization on GaAs(100) using Electron cyclotron resonance or Glow discharge N_2 plasma sources for the nitriding process

H. Mehdi[1], F. Réveret[1], C. Bougerol[2], C. Robert-Goumet[1], P. E. Hoggan[1], L. Bideux[1], B. Gruzza[1], J. Leymarie[1], G. Monier[1]

[1]*Université Clermont Auvergne, CNRS, SIGMA Clermont, Institut Pascal, F-63000 CLERMONT-FERRAND, France*
[2]*Université Grenoble Alpes, CNRS, Institut Néel, 38000 GRENOBLE, France*

* Corresponding author. Tel.: +33 473 407 118. E-mail address: guillaume.monier@uca.fr.

Abstract:

Two kinds of N_2 plasma source, ECR (electron cyclotron resonance) and GDS (glow discharge source) generating mostly N-radical atoms and N-cationic species respectively, were used to grow a thin nitride layer on a GaAs(100) substrate. It was found that this nitridation followed by annealing at 620°C permits the crystallization of the nitride layer. Pyramidal Zinc Blende GaN nanostructures (zb-GaN) with four facets were obtained using GDS plasma. Surprisingly, a planar and pure Wurtzite structure (w-GaN) was obtained using the ECR source. This w-GaN structure shows low photoluminescence intensity and a biaxial tensile strain due to lattice mismatch. Accordingly, the operator can select which phase is formed, simply by switching plasma source. The valence band discontinuity ΔE_v has been determined to be 1.74 eV for the zb-GaN/GaAs and w-GaN/GaAs junctions by X-ray photoelectron spectroscopy. As a consequence the conduction bands of the GaAs substrate and the elaborated GaN thin layer are aligned for a zb-GaN/GaAs junction giving efficient electron transport at the zb-GaN/GaAs interface. For w-GaN/GaAs junction, the conduction band discontinuity ΔE_c is 0.23 eV inducing an electron confinement in the GaAs(100) which can be an effective way to improve the electronic or optical properties of GaAs devices.

1. Introduction

III-V compound semiconductors are mandatory for the development of high performance electronic and optoelectronic devices. In particular, GaAs semiconductors are employed in a variety of applications such as light emitting diodes (LEDs)[1], laser diodes (LDs)[2], high speed communication[3], photodetectors[4], photovoltaics[5], gas sensors[6] and nanomechanical resonators[7]. Nevertheless, the GaAs surface has a low electronic and optical quality due to the presence of high densities of surface states induced by the native oxide formation at the surface. These states act as non-radiative recombination centers causing Fermi level pinning near GaAs surfaces which reduces the performance of GaAs-based devices.

Therefore, surface passivation is one of the most important aspects when developing GaAs-based devices, especially since the dimensions of these currently decrease, making surface properties become increasingly important. With this in mind, different surface passivation techniques have been studied in recent years[8][9][10] and the most used passivating process nowadays is the epitaxial growth of AlGaAs or InGaP layer[11][12]. Nevertheless, the different techniques come up against many problems, such as progressive degradation from air and light exposure[13][14][15]. In our view, particularly considering the case of nanostructures (nanowires, nanodots, etc…), the nitridation process seems to be very adaptable[16][17][18]. In this way, plasma passivation using very low power N_2 plasma sources may prove to be a suitable process, providing chemically and thermally stable ultra-thin passivating layer on GaAs(100) surface[19][20]. Indeed, GaN layer is less susceptible to environmental oxidation and, as we will demonstrate, provides thermal stabilization of the GaAs surface, up to 670°C. Moreover, the GaN layer has a high band gap giving a barrier to confine electrons in GaAs substrate which can be useful in light-emitting and photo-voltaic applications.

Thus, in this work, we focused our attention on elaboration of a well-controlled ultra-thin film of GaN on GaAs(100), showing well-ordered crystalline structures and thermal stability. Especially, we study the influence of the nature of nitrogen species produced during nitridation on the GaN structure. Indeed, GaAs(100) substrates are nitrided using two different N_2 plasma sources running at very low power (<30 W), an electron cyclotron resonance source (ECR) and a glow discharge source (GDS), generating mostly radical N atoms and cationic nitrogen species respectively. Using low energy electron diffraction (LEED) and transmission electron

© 2019 published by Elsevier. This manuscript is made available under the CC BY NC user license
https://creativecommons.org/licenses/by-nc/4.0/

microscopy (TEM), we will show that the nitridation followed by annealing at 620°C, permits the crystallization of the GaN layer into the Wurtzite (w-GaN) or Zinc Blende (zb-GaN) structure depending on which plasma N_2 source is used. This opens the possibility of selective phase formation. Optical properties of the elaborated GaN thin layer will be highlighted by photoluminescence measurements. Moreover, the band offset at the GaN/GaAs heterojunction will be determined by measuring the valence band discontinuity for the GaN/GaAs junctions using X-ray photoemission spectroscopy giving a vertical contact scheme primordial for GaAs based Schottky diodes[21].

2. Experimental

HCl-isopropanol chemical solution was used to clean the GaAs(100) substrates[22]. This reduces the damage of the surface compared to the classical ion bombardment. Then, the substrate is transferred rapidly under vacuum to reduce the surface re-oxidation. The GaAs samples were heated at 530°C to remove all re-adsorbed molecules and the Ga rich (4×1) reconstruction was observed on LEED patterns. Nitridation was performed at 25, 400 and 500°C using a N_2 plasma produced by a homemade glow discharge source (GDS) described in detail in Ref.[23] and a commercial electron cyclotron resonance source (SPECS MPS-ECR) operating in atom mode at a pressure of 10^{-2} Pa for different nitridation times as shown in Table 1. For the GDS source a high DC voltage of 2.5 kV is applied between an anode which is a stainless steel cylinder and cathode linked to the preparation chamber connected to earth providing a discharge. This discharge is responsible for cracking the N_2 molecule generating a high flux of positive nitrogen ions only at a pressure below 4×10^{-2} Pa. The density current on the sample is 1 $\mu A/cm^2$ and the source power is estimated at 5 W. For the ECR source, a microwave magnetron generates microwaves, with a frequency of 2.45 GHz and a power around 30 W, arriving in a discharge chamber where a sophisticated magnetic field is created by a magnetic quadrupole producing an electron cyclotron resonance mechanism. This mechanism with a high local N_2 gas pressure excites a plasma with a high density due to the spiralling motion of the electrons. Low conductance boron nitride plates with several small holes are placed at the open end of the discharge chamber to prevent ions nitrogen from leaving the source. Using this source, a majority of radical N atoms arrive at the GaAs surface inducing a current density on the sample of 12 nA/cm^2. After nitridation, all samples are annealed at 620°C for 1 h.

X-ray photoelectron spectroscopy (XPS) measurements were carried out in a UHV chamber equipped with a dual anode Al-Mg X-ray source and hemispherical electron energy analyzer OMICRON EA 125 where are separated by an angle of 55° (almost the "magic angle": L=1). The Mg Kα (1253.6 eV) photons and a constant pass energy of the analyzer equal to 20 eV were used for analysis. The elaborated GaN thin layer thicknesses were determined using the XPS model reported in Ref.[20]. In this reference, the GaAs nitridation process is developed including the GaAs nitridation steps and a kinetic model giving the kinetic growth parmeters of the process.

Photoluminescence (PL) measurements were performed at low temperature 5 K using a liquid helium circulation cryostat. The elaborated GaN thin layer was excited by the continuous 325 nm wave line of a He-Cd UV laser with a power density of 640 W/cm^2. The emitted light is focused on the monochromator slit and detected by a CCD camera system having an energy resolution of 0.6 nm.

3. Results and discussion

A. Nitridation with GDS source: zb-GaN structure

Before annealing, the elaborated GaN samples do not show any crystalline structure (no LEED pattern). Thus, the GaN thin layers are amorphous, however previous work has shown that it is possible to crystallize the GaN layer after annealing at 620°C[19]. The LEED patterns taken with an incident electron energy of 57, 59, 63 and 65 eV for the G1 sample are shown in Figure. 1. In this figure, the variation of the incident electron energy even of just 1 eV induces substantial shifting of the diffraction points and not all with the same direction. Indeed, the lighted points surrounded by red and blue circles move along two lines x and y. The red circles diverge towards the outside of the LEED pattern while the blue ones converge to the LEED pattern center. This observation is not consistent with all diffraction patterns obtained on a flat surface. Several research groups have made similar observations and explain that this shift is caused by crystallite facet formation[24]. To determine the facet

characteristics, we use the method described by Yang *et al.*[25] providing accurate results since several LEED patterns at different energies are used.

A illustration of a crystallite facet I on GaAs(100) surface is presented in Fig. 2 where $\overrightarrow{k_0}$ and $\overrightarrow{k_1}$ are respectively the incident and the diffracted electron wave vectors, α is the diffraction angle, θ is the inclination angle between the facet I and the GaAs(100) surface. The Laue condition (diffraction condition) is given in Eq. 1.

$$\overrightarrow{d}.\overrightarrow{s_1} - \overrightarrow{d}.\overrightarrow{s_0} = n\lambda,$$

$$d.sin(\alpha - \theta) - d.sin(\theta) = n\lambda \quad (1)$$

where $\overrightarrow{k_0}$ and $\overrightarrow{k_1}$ are the unit vectors of the incident and the diffracted electrons respectively, d is the interreticular distance in the facet I, n is the order number of the diffraction electrons and λ is the wavelength of the incident electrons. The momentum transfer vector is given by $\Delta\vec{K} = \overrightarrow{k_1} - \overrightarrow{k_0}$. The parallel and perpendicular components of the momentum transfer $\Delta K_{\parallel}$ and $\Delta K_{\perp}$are expressed in Eq.(2) and Eq.(3) respectively.

$$\Delta K_{\parallel} = k_0.sin(\alpha) \quad (2)$$

$$\Delta K_{\perp} = k_0.cos(\alpha) + k_0 \quad (3)$$

where k_0 and k_1 are the incident and diffracted electron wave vector magnitudes, here $k_0 = k_1$ since only elastic diffracted electrons are considered. Injecting the expression of $sin(\alpha)$ and $cos(\alpha)$ from Eq.(2) and Eq.(3) respectively in Eq(1), the relation between $\Delta K_{\parallel}$ and $\Delta K_{\perp}$is obtained in Eq.(4) which allows the angle θ between the facet I and GaAs(100) surface to be determined.

$$\Delta k_{\parallel} = tan(\theta).\Delta k_{\perp} + \frac{2\pi.n}{d.cos(\theta)} \quad (4)$$

For each point lit surrounded by a circle in Fig. 1, the components of the momentum transfer using respectively Eq.(2), Eq.(3) once the diffraction angle α are determined.

In Figs. 3a, 3b, 3c and 3d, we show respectively the variation of $\Delta K_{\parallel}$ as function of the $\Delta K_{\perp}$ for each couple of points $(a_1^*; b_1^*)$, $(a_2^*; b_2^*)$, $(a_3^*; b_3^*)$ and $(a_4^*; b_4^*)$ noted in Fig. 1. In these figures, lines represent the best fits obtained using Eq.(4) allowing the determination of the angle θ and the lattice parameter for each point surrounded by circle by considering a diffraction order value of 3 for $(a_2^*; b_2^*)$, $(a_4^*; b_4^*)$ and -3 for $(a_1^*; b_1^*)$, $(a_3^*; b_3^*)$ as listed in Table 2. As this table shows, the average values of the inclination angle θ are 44.5°, -44.8°, 134.7° and -134° for $(a_1^*; b_1^*)$, $(a_2^*; b_2^*)$, $(a_3^*; b_3^*)$ and $(a_4^*; b_4^*)$ respectively with an uncertainty estimated at 3°. These angles are consistent with the inclination angle of the facets (110), (1-10), (-110) and (-1-10). Furthermore, the values of the calculated lattice parameters $(a_1; b_1)$, $(a_2; b_2)$, $(a_3; b_3)$ and $(a_4; b_4)$ collected in Table 2 having average values of (4.43 Å; 3.19 Å) and are very close to (4.50 Å; 3.18 Å) which are reported in the literature for a fully relaxed zb-GaN[26]. Note that for any incident electron energy the a_i^* and b_i^* points with i ϵ ℕ are always perpendicular. Consequently, we conclude the formation of four cubic GaN facets with (110), (1-10), (-110) and (-1-10) orientations. Moreover, since the diffraction points are conserved under C4 rotation, these four cubic facets can form pyramidal GaN nanostructures with a square base. Same results are obtained for the G2 sample. The LEED patterns of the G3 sample present weak spot light intensity which can be related to the high GaN thicknesses involving formation of few GaN crystallites.

These results are consistent with the scanning electron microscopy (SEM) image of the G1 sample presented in Fig. 4a which shows a homogeneous distribution of the GaN nanostructures on the surface. When we increase the magnification to identify the shape of these nanostructures, we cannot obtain a clear image due to the insulating character of the GaN material. For the G3 sample, there are fewer GaN nanostructures formed on the surface as shown in Fig. 4b. This observation can be explained by the highest GaN thickness obtained for G3 sample for which the morphology of these nanostructures is not well defined.

A photoluminescence (PL) investigation of G1, G2 and G3 samples is performed. The PL spectrum related to G2 shown in Fig. 5 is dominated by a neutral donor-band transition D^0h at 3.22 eV. The donor-acceptor pair DAP

transition is observed at 3.15 eV. These two values are consistent with the transition energies observed in a totally relaxed Zinc Blende GaN[27][28]. Such relaxation explains that pyramid-nanostructures are observed after annealing at 620°C. The required crystallite formation energy is reduced by relaxation to compensate the large lattice mismatch between zb-GaN and GaAs(100) of 20%. The emission located at low energy cannot be ascribed to the DAP phonon replica since its intensity is higher than that of the DAP transition. To explain this transition, Wu *et al.*[29] have suggested an emission at 3.056 eV related to the recombination between an electron and an additional neutral acceptor. Another work by Xu *et al.*[28] confirms that the emission at 3.081 eV is due to the recombination between an electron and a neutral acceptor eA^0 by studying the energy transition dependence as function of the temperature. Therefore, the emission at 3.06 eV corresponds probably to an electron-neutral acceptor recombination. Moreover, no PL spectrum was observed for G1 and G3 samples. The low GaN crystallite size in the sample G1 characterized by a high surface/volume ratio induces many non-radiative centers which reduce the possibility of obtaining a PL signal. The low GaN crystalline quality for the G3 sample as seen in Fig. 4b explains the absence of PL spectrum. Therefore, the GaN thickness and its crystalline quality are two essential parameters to obtain a PL spectrum.

B. Nitridation with ECR source: w-GaN structure

In this section, we identify the structure of the GaN elaborated by the MPS-ECR source for the E2 and E3 samples. As for the samples nitridated with a GDS source, the LEED measurements were made on the samples E1, E2 and E3 nitrided with the ECR source as detailed in Table 1. The LEED patterns corresponding to E2 and E3 samples presented in Figs. 6a, 6b respectively show that the GaN thin layer has a hexagonal structure (w-GaN). These LEED patterns are centro-symmetric by changing the electron energy and remain the same by shifting the analyzed surface which shows a flat GaN structure on all the sample surface. The background noise in the LEED pattern for E2 (Fig. 6a) is greater than for E3 which can be related to the w-GaN low crystalline quality. Note that the GaN thin layer elaborated at 25°C (E1) is not crystallized since no LEED pattern was observed. Then, the nitridation temperature plays a crucial role to obtain a high quality of w-GaN. Indeed, previous work[20] shows that, at low nitridation temperature (T<500°C), the inter-diffusion of nitrogen and arsenic atoms induces a small quantity of free arsenic remaining in the GaN thin layer. This quantity of free arsenic could prevent the w-GaN structuration.

Further analyses of the w-GaN/GaAs(100) interface roughness were performed by high-resolution transmission electron microscopy (HR-TEM) on the E3 sample. A cross sectional HR-TEM image of the sample oriented along the [01-1] GaAs zone axis (confirmed by the FFT of the image in inset) is given in Fig. 7a. A zoom of the image presented in Fig. 7b shows the presence of a thin GaN layer in the [10-10] orientation, as evidenced by the FFT in the inset, with an abrupt interface with the GaAs(100) substrate. In this image, there is no evidence of GaAs(111) facet formation at the interface which promotes the nucleation of hexagonal GaN structure as reported in Refs.[30][31]. To our knowledge, it is the first time that a hexagonal GaN structure is obtained directly on GaAs(100). Tsuchiya *et al.*[32] show that the hexagonal phase of GaN is dominant during GaN growth on GaAs(100) by HVPE using a high V/III ratio. Therefore, the w-GaN structure obtained in our work can be explained by nitrogen excess in the GaN layer caused by the low radical nitrogen diffusion as it was shown previously in Ref.[20]. Another benefit of the GaAs(100) nitridation using ECR plasma source is getting an abrupt interface between w-GaN and GaAs substrate whereas Tsuchiya *et al.*[32] obtain GaAs(111) facet formation showing a high interface roughness. Note also that the interface of the zb-GaN/GaAs(100) heterojunction obtained using GDS source and reported in a previous work[19], is rougher than the w-GaN/GaAs(100) interface.

The determined in-plane lattice constant a of w-GaN for E2 and E3 samples is respectively 3.26 and 3.28 Å with an accuracy of 0.06 Å. These values are higher than that reported in the literature for a relaxed w-GaN of 3.19Å[33]. It indicates that there is a tensile strain in the w-GaN thin layer induced by the GaAs(100) substrate. To get more information about the w-GaN layer strain, the PL spectrum for the E3 sample is displayed in Fig. 8 and reveals two emissions at 3.42 and 3.20 eV. As a comparison, for a totally relaxed w-GaN, the neutral donor-exciton D^0X transition is localized in a region between 3.466 and 3.476 eV[34][35] which is far from the measured value of 3.42 eV. Thillosen *et al.*[36] explain that the D^0X energy shifts towards the low energy side are characteristic of the w-GaN under tensile strain; this result is consistent with the LEED results. The emission at 3.42 eV can be ascribed to the D^0X_B transition since the transition related to exciton A or C is above this energy for the tensile strain case as shown in Ref.[37]. The second emission at 3.20 eV is related to the donor-

acceptor pair DAP transition. It is also shifted towards lower energy compared to the value obtained of 3.25 eV for the fully relaxed w-GaN[34]. This result is also consistent with the LEED measurement where the determined in-plane w-GaN lattice constant a is dilated compared to the value reported in the literature for a totally relaxed w-GaN layer.

To estimate the importance of this tensile strain in the w-GaN ultra-thin layer, the tensor component ϵ_{zz} was determined using Eq.(11) presented in Ref.[38] where the biaxial strain dependence of exciton energies is studied. The energy expression of the valence band state of Γ_{7V} symmetry for a strained wurtzite structure given in Ref.[39] which corresponds to exciton B was injected into this equation. The energy of exciton B was expected 6 meV above the D^0X_B transition at a value of 3.426 eV. This value and all constants reported in Refs.[38][40] used for calculation of ϵ_{zz} yield -2.5×10^{-3} for ϵ_{zz}. As we have considered that the valence band energy near$\Gamma_{7V}$is under biaxial strain, the relation $\epsilon_{xx} = \epsilon_{yy} = (-C_{33}/2.C_{13})\epsilon_{zz}$ where C_{ij} are elastic stiffness constants, i.e components of the related tensor calculated for w-GaN in Ref.[40] can be used and a value of 4.2×10^{-3}, for the two tensor components ϵ_{xx} and ϵ_{yy} is found. These tensor component values confirm that the elaborated w-GaN exhibits an in-plane biaxial tensile strain.

Considering these results, regardless of the use of the GDS or ECR source, one can note the thermal stabilization of GaAs surface by a thin film of GaN. Indeed, the GaAs can be heated up to 620°C without the need of an As flux stabilization. This observation was corroborated by thermostated Car-Parrinello dynamics. A slab periodic structure, as previously used exposes the (100) face of GaAs in the zinc-blende structure[41]. This undergoes a temperature ramp and the onset of movement compatible with melting occurs at 530°C which is consistent with Ref.[42]. Two mesh of GaN are then added and the onset of melting occurs at 670°C (experimentally, the decomposition of the surface was observed at 650°C (not shown here)).

C. Band offset of GaN/GaAs

The valence band discontinuity at the GaN/GaAs(100) heterojunction interface was measured using the method described in Ref.[43] based on XPS measurements. It can be calculated by Eq.(5)

$$\Delta E_v = (E_{VBM} - E_{As3d})^{GaAs} - (E_{VBM} - E_{Ga3d})^{GaN} - \Delta E_{Ga3d-As3d}^{GaN/GaAs} \quad (5)$$

where $(E_{VBM} - E_{As3d})^{GaAs}and(E_{VBM} - E_{Ga3d})^{GaN}$are the core-level energy of $As3d_{5/2}$ and $Ga3d_{5/2}$ determined with respect to the valence band maximum for pure GaAs and GaN, respectively and $\Delta E_{Ga3d-As3d}^{GaN/GaAs}$ is the core-level separation between $Ga3d_{5/2}$ and $As3d_{5/2}$ for the GaN/GaAs heterojunction sample.

For a cleaned GaAs substrate, the separation between the core-level energy of $As3d_{5/2}$ and VBM is measured to be 40.67 ± 0.1 eV. Note that, due to the very low GaN thickness elaborated using GDS or ECR sources[20], the GaN layer cannot be considered as bulk. Therefore, the reference $(E_{VBM} - E_{Ga3d})^{GaN}$ was measured for a commercial w-GaN(0001) substrate at 17.70 eV. This value is used only for E2 and E3 where the w-GaN structure is observed. While for G1, G2 and G3 samples having a zb-GaN structure, the value of 17.66 eV reported in Ref.[44] for cubic GaN grown by MBE (Molecular beam epitaxy) was used. In addition, the core-level separation between $Ga3d_{5/2}$ and $As3d_{5/2}$ across the GaN/GaAs interface was determined by XPS at 21.23 eV for E2 and E3 and at 21.27 eV for G1, G2 and G3 samples. The latter value is very close to the one determined in Ref.[44] at 21.30 eV. Taking into account the uncertainty of our XPS measurement of 0.1 eV, the difference between these two values is not significant. Therefore, the measured valence band discontinuity ΔE_v for the w-GaN/GaAs(100) and zb-GaN/GaAs(100) heterojunctions is 1.74 ± 0.1 eV. This value indicates that the holes are localized in the GaAs substrate for these two heterojunctions and must exceed a potential barrier of 1.74 eV to cross the GaN/GaAs interfaces.

In order to determine the conduction band discontinuity ΔE_c for these two heterojunctions, the values of the band gap energy of the elaborated zb-GaN and w-GaN thin layers and of the GaAs substrate at 300 K must be obtained. Based on PL spectrum presented in Figs. 5 and 8, value of 3.45 eV (3.30 eV) for w-GaN (zb-GaN) thin layers were calculated by adding 25 meV (52 meV) above the D^0X_B (D^0h) to determine the free exciton transition energy, and 6 meV (28 meV) to obtain the band gap energy at 5 K. A value of 1.51 eV was considered for the band gap energy at 5 K of the GaAs substrate[45]. Using the empirical equation of Varshni[46] and the

constants obtained from Refs.[47][48][49], a band gap energy at 300 K of 3.23, 3.38 and 1.41 eV for zb-GaN and w-GaN thin layers and GaAs substrate can be calculated respectively. These values for GaAs substrate and zb-GaN are in good agreement with those reported in the literature[50][51] while the value of the band gap energy for w-GaN is lower than that given by Ref.[52] for bulk w-GaN due to the tensile strain effect in the w-GaN thin layer. Hence, the value of ΔE_c is equal to 0.08 and 0.23 eV for zb-GaN/GaAs (G2) and w-GaN/GaAs (E3) heterojunctions respectively. The schematic representations of band alignment are presented in Fig. 9. For zb-GaN/GaAs heterojunction, the maxima of the conduction band for GaAs and thin zb-GaN layer can be considered aligned since the ΔE_c is lower than the uncertainty of the XPS measurement (0.1 eV). This therefore provides a good electron transport across the zb-GaN/GaAs interface. For w-GaN/GaAs junction, the electrons need to reach a barrier height of 0.23eV to pass across the interface. In this case, the electrons are confined in the GaAs substrate which can increase its photoluminescence efficiency.

4. Conclusion

Using cationic nitrogen species (GDS source) during GaAs(100) nitridation has shown the formation of a relaxed pyramidal GaN nanostructure (with square base) where its four facets have a cubic structure oriented (110), (1-10), (-110) and (-1-10) for GaAs(100). While a planar hexagonal GaN structure substrate has been obtained when mostly radical nitrogen atoms (ECR source) were used showing an abrupt interface between the w-GaN thin layer and GaAs(100). Consequently, the nature of the nitrogen species used during nitridation has a direct impact on the GaN structuration after a crystallization at 620°C. Accordingly, the operator can select which phase is formed, simply by switching plasma source. To our knowledge, this is the first time that a hexagonal GaN structure was obtained on GaAs(100) without using a gallium precursor or a nucleation layer. This hexagonal GaN thin layer can passivate the GaAs surface and also act as a buffer layer to grow hexagonal structure layers by epitaxy such as AlN for microelectronics applications. w-GaN/GaAs and zb-GaN/GaAs heterojunctions have the same valence band discontinuity having a value of 1.74 eV. Conversely, the conduction band discontinuity for w-GaN/GaAs is larger than that for zb-GaN/GaAs inducing the confinement of electrons in the GaAs substrate which can improve its electrical and optical properties raising the performance of GaAs-based devices.

References

[1] K. Chen, T. P. Xiao, P. Santhanam, E. Yablonovitch, and S. Fan, Journal of Applied Physics 122, 143104 (2017)

[2] Z. Qiao, X. Tang, X. Li, B. Bo, X. Gao, Y. Qu, C. Liu and H. Wang, IEEE Journal of the Electron Devices Society 5, 122 (2017)

[3] B. Curran, J. Reyes, C. Tschoban, J. Höfer, A. Grams, F. Wüst, M. Hutter, J. Leiß, M. Martínez-Vázquez, R. Baggen, I. Ndip and K. Lang, IEEE Transactions on Components Packaging and Manufacturing Technology 8, 1231 (2018)

[4] S. H. Kim, D. M. Geum, M. S. Park, H. S. Kim, J. D. Song, and W. J. Choi, Applied Physics Letters 110, 153505 (2017)

[5] J. Fakidis, S. Videv, H. Helmers and H. Haasi, IEEE Photonics Technology Letters 30, 841 (2018)

[6] Q. Clément, J. -M. Melkonian, J. -B. Dherbecourt, M. Raybaut, A. Grisard, E. Lallier, B. Gérard, B. Faure, G. Souhaité and A. Godard, Optics Letters 40, 2676 (2015)

[7] H. Yamaguchi, Semiconductor Science and Technology 32, 103003 (2017)

[8] R. Roychowdhury, V. K. Dixit, G. Vashisht, T. K. Sharma, C. Mukherjee, S. K. Rai and S. Kumar, Applied Surface Science 476, 615 (2019)

[9] X. Huang, P. Xia, X. Wang and Y. Hu, Applied Surface Science 473, 141 (2019)

[10] L. Zhou, B. Bo, X. Yan, C. Wang, Y. Chi and X. Yang, Crystals 8, 226 (2018)

[11] X. Yuan, L. Li, Z. Li, F. Wang, N. Wang, L. Fu, J. He, H. Hoe Tanb and C. Jagadish, Nanoscale 11, 9207 (2019)

[12] G. K. Dalapati, C. K. Chia, C. C. Tan, H. R. Tan, S. Y. Chiam, J. R. Dong, A. Das, S. Chattopadhyay, C. Mahata, C. K. Maiti and D. Z. Chi, ACS Applied Materials & Interfaces 5, 949 (2013)

[13] Y. Wang, Y. Darici, and P. H. Holloway, Applied Physics Letters 54, 724 (1989)

[14] A. Jaouad, V. Aimez, Applied Physics Letters 89, 092125 (2006)

[15] C. Edirisinghe, H. E. Ruda, I. Koutzarov, Q. Liu, L. Jedral, M. G. Boudreau, M. Boumerzoug, J. Brown, P. Mascher, A. Moore, R. Henderson, Mat. Res. Soc. Symp. Proc. 54, 378 (1995)

[16] H. J. Chen, Y. Su, D. Yang, T. Huang, I. Yu, Surface & Coatings Technology 324, 491 (2017)

[17] P. A. Alekseev, M. S. Dunaevskiy, V. P. Ulin, T. V. Lvova, D. O. Filatov, A. V. Nezhdanov, A. I. Mashin, and V. L. Berkovits, Nano Letters 15, 63 (2015)

[18] M. Mamizuka, O. Kojima, T. Inoue, T. Kita, O. Wada, Phys. Status Solidi 6, S-146 (2009)

[19] G. Monier, L. Bideux, C. Robert-Goumet, B. Gruzza, M. Petit, J. L. Lábár, M. Menyhárd, Surface Science 606, 1093 (2012)

[20] H. Mehdi, G. Monier, P. E. Hoggan, L. Bideux, C. Robert-Goumet and V. G. Dubrovskii, Applied Surface Science 427, 662 (2018)

[21] A. H. Kacha, B. Akkal, Z. Benamara, M. Amrani, A. Rabhi, G. Monier, C. Robert-Goumet, L. Bideux, B. Gruzza, Superlattices and Microstructures 83, 827 (2015)

[22] O. E. Tereshchenko, S. I. Chikichev, and A. S. Terekhov, Journal of Vaccum Science Technology A. 17, 2655 (1999)

[23] V. Matolín, S. Fabík, J. Glosík, L. Bideux, Y. Ould-Metidjib and B. Gruzza, Vacuum 76, 471 (2004)

[24] Charles W. Tucker Jr, Journal of Applied Physics 38, 1988 (1967)

[25] Y. Yang and E. D. Williams, Journal of Vacuum Science & Technology A. 8, 2481 (1990)

[26] X. H. Zhenga, Y. T. Wanga, Z. H. Fenga, H. Yanga, H. Chenb, J. M. Zhoub and J. W. Lianga, Journal of Crystal Growth 250, 345 (2003)

[27] J. Menniger, U. Jahn, O. Brandt, H. Yang, and K. Ploog, Physical Review B 53, 1881 (1996)

[28] D. Xu, H. Yang, J. B. Li, D. G. Zhao, S. F. Li, S. M. Zhuang, R. H. Wu, Y. Chen and G. H. Li, Applied Physics Letters 76, 3025 (2000)

[29] J. Wu, H. Yaguchi, K. Onabe, R. Ito, and Y. Shiraki, Applied Physics Letters 71, 2067 (1997)

[30] S. Huang, H. Wang, C. Hsu, J. Gong, C. Chiang, S. Tu and H. Chang, Journal of Materials Science Letters 17, 1281 (1998)

[31] A. Kikuchi, H. Hoshi and K. Kishino, Japanese Journal of Applied Physics 33, 688 (1994)

[32] H. Tsuchiya, K. Sunaba and S. Yonemura, Japanese Journal of Applied Physics 36, L1 (1997)

[33] M. Leszczynski, H. Teisseyre, T. Suski, I. Grzegory, M. Bockowski, J. Jun, S. Porowski, K. Pakula, J. M. Baranowski, C. T. Foxon and T. S. Cheng, Applied Physics Letters 69, 73 (1996)

[34] J. Menniger, U. Jahn, O. Brandt, H. Yang, and K. Ploog, Physical Review B 53, 1881 (1996)

[35] M. Mayer and A. Pelzmann, M. Kamp, K. J. Ebeling, H. Teisseyre, G. Nowak, M. Leszczyński, I. Grzegory, S. Porowski and G. Karczewski, Japanese Journal of Applied Physics 36, L1634 (1997)

[36] N. Thillosen, K. Sebald, H. Hardtdegen, R. Meijers, R. Calarco, S. Montanari, N. Kaluza, J. Gutowski, and H. Lüth, Nano Letters 6, 704 (2006)

[37] S. Chichibu, T. Azuhata, T. Sota, H. Amano, and I. Akasaki, Applied Physics Letters 70, 2085 (1997)

[38] A. Shikanai, T. Azuhata, T. Sota, S. Chichibu, A. Kuramata, K. Horino and S. Nakamura, Journal of Applied Physics 81, 417 (1997)

[39] B. Gil, O. Briot, and R. Aulombard, Physical Review B 52, 28 (1995)

[40] K. Shimada, T. Sota and K. Suzuki, Journal of Applied Physics 84, 4951 (1998)

[41] G. Monier, P. Hoggan, L. Bideux, D. Paget, H. Mehd, S. Kubsky, P. Dumas and C. Robert-Goumet, Applied Surface Science 465, 787 (2019)

[42] A. A. Spirina, A. G. Nastovjak, N. L. Shwartz, J. Phys.: Conf. Ser. 993, 012011 (2018)

[43] E. A. Kraut, R. W. Grant, J. R. Waldrop, and S. P. Kowalczyk, Physical Review Letters 44, 1620 (1980)

[44] S. A. Ding, S. R. Barman, K. Horn, H. Yang, B. Yang, O. Brandt, and K. Ploog, Applied Physics Letters 70, 2407 (1997)

[45] E. Grilli, M. Guzzi, R. Zamboni, and L. Pavesi, Physical Review B 45, 1638 (1992)

[46] Y. P. Varshni, Physica 34, 149 (1967)

[47] W. Shan, T. Schmidt, X. H. Yang, J. J. Song, and B. Goldenberg, Journal of Applied Physics 79, 3691 (1996)

[48] R. Liu and C. Bayram, Journal of Applied Physics 120, 025106 (2016)

[49] E. Grilli, M. Guzzi, R. Zamboni, and L. Pavesi, Physical Review B 45, 1638 (1992)

[50] M. El Allali, C. B. Sørensen, E. Veji, and P. Tidemand-Petersson, Physical Review B 48, 4398 (1993)

[51] G. Ramírez-Flores, H. Navarro-Contreras, A. Lastras-Martínez, R. C. Powell, and J. E. Greene, Physical Review B 50, 8433 (1994)

[52] B. Monemar, Applied Physics Letters 10, 676 (1974)

Table 1 Nitridation parameters of GaAs (100) substrate by GDS and ECR sources and the corresponding estimated GaN thicknesses. All samples are annealed at 620°C.

Sample	Source	Temperature (°C)	t (min)	GaN thickness (nm)
G1	GDS	25	5	1
G2	GDS	400	23	1.5
G3	GDS	500	60	2.9
E1	ECR	25	180	1.1
E2	ECR	400	60	1.7
E3	ECR	500	60	2.3

Table 2 Characteristic parameters of zb-GaN facets formed on GaAs(100).

Couple	tan θ	$\theta_{measured}$	Lattice parameter Å	Ordre n	Orientation
$(a_1^*; b_1^*)$	(0.91;1.04)	(42.9° ; 46.1°)	$(a_1 = 4.55; b_1 = 3.18)$	-3	(1 1 0)
$(a_2^*; b_2^*)$	(-0.99;-1.00)	(-44.7° ; -45°)	$(a_2 = 4.37; b_2 = 3.31)$	3	(1 -1 0)
$(a_3^*; b_3^*)$	(-1.00;-1.02)	(135.0° ; 134.4°)	$(a_3 = 4.37; b_3 = 3.22)$	-3	(-1 1 0)
$(a_4^*; b_4^*)$	(1.00;1.07)	(-135.0° ; -133.0°)	$(a_4 = 4.44; b_4 = 3.08)$	3	(-1 -1 0)

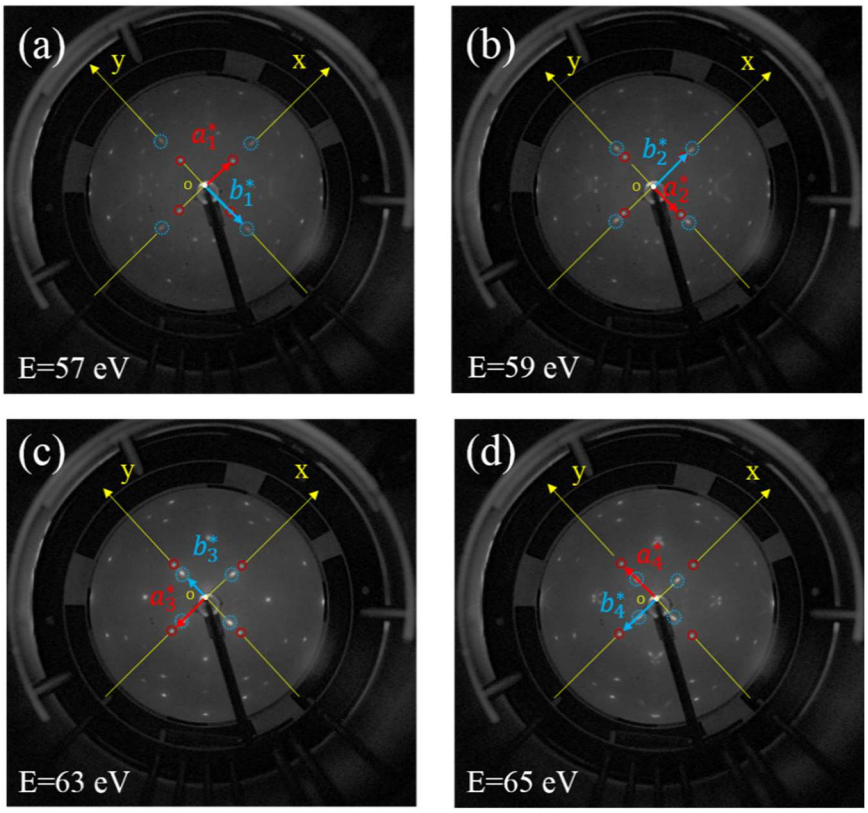

Figure 1 LEED patterns for G1 sample taken at different incident electron energy of 57, 59, 63 and 65 eV.

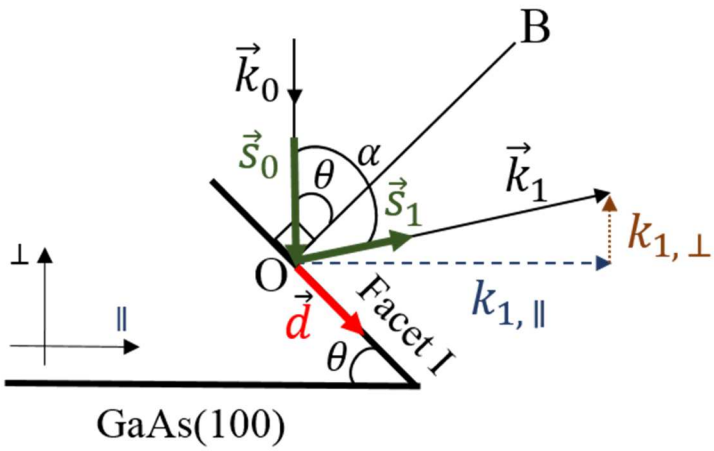

Figure 2 Schematization of a crystallite facet I on GaAs (100) surface. OB is the normal to the facet I surface.

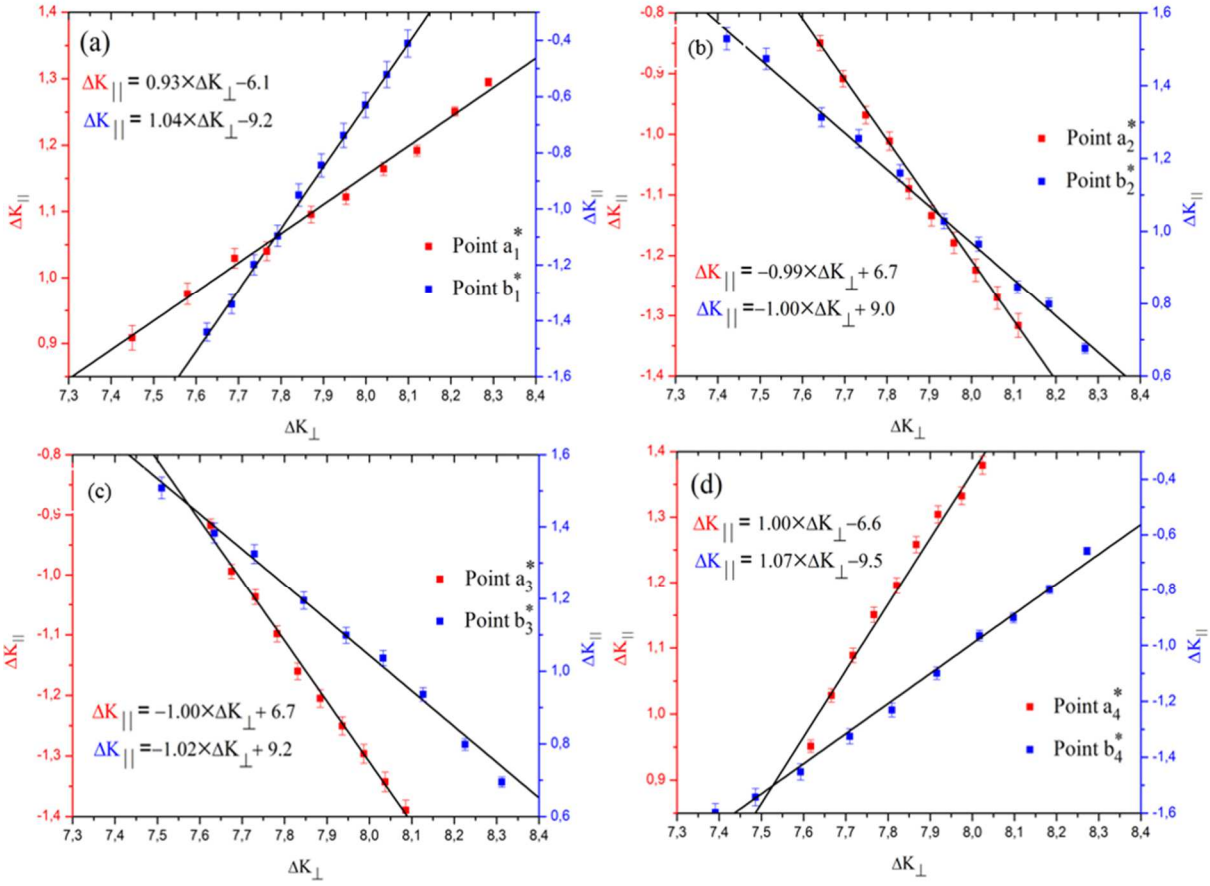

Figure 3 Parallel momentum transfer versus perpendicular momentum transfer for each lighted point present in Fig. 1. Lines are the best fits using Eq.(4).

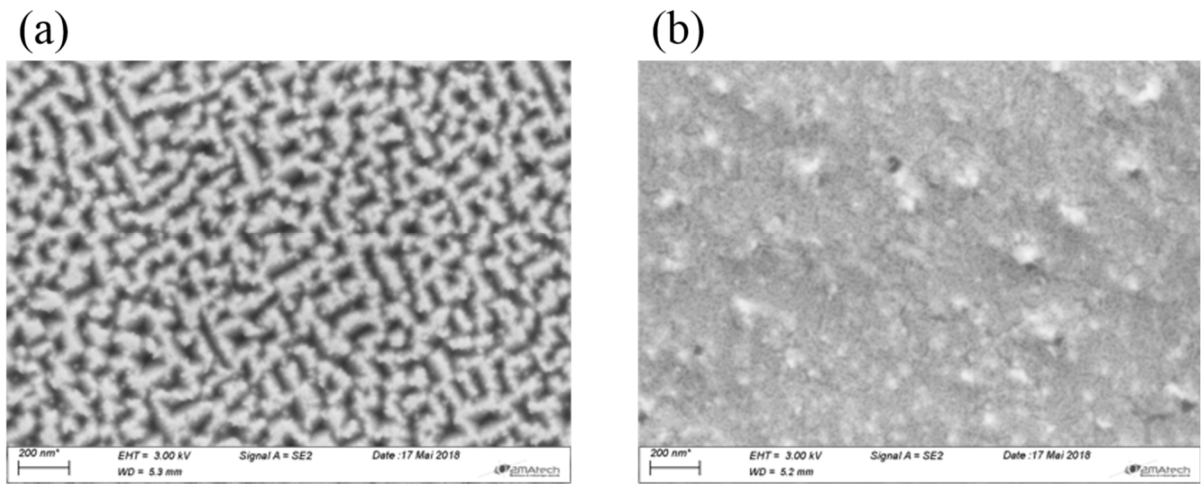

Figure 4 SEM image of the GaN surface for (a) G1 and (b) G3.

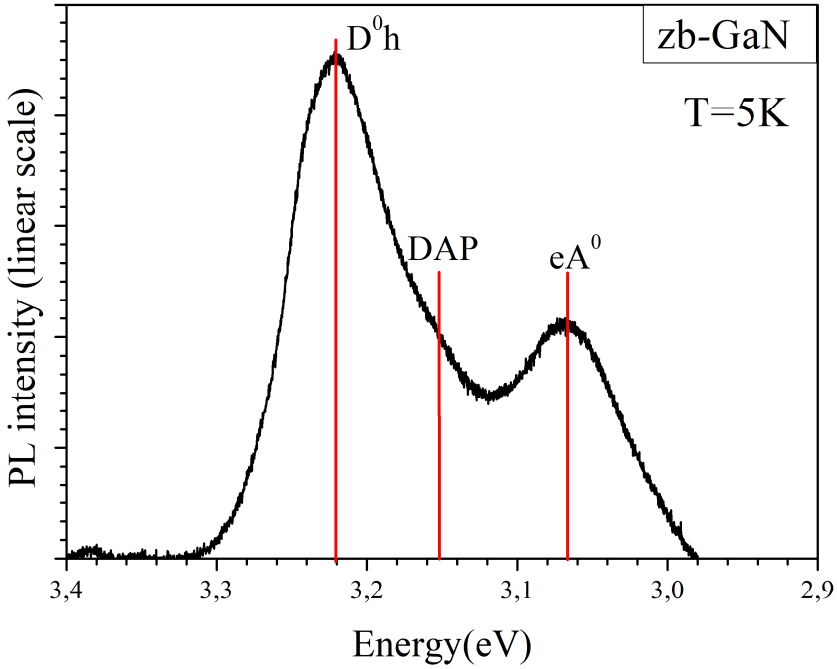

Figure 5 Photoluminescence spectrum for G2 sample recorded at T=5K with a power density of 640 W/cm^2.

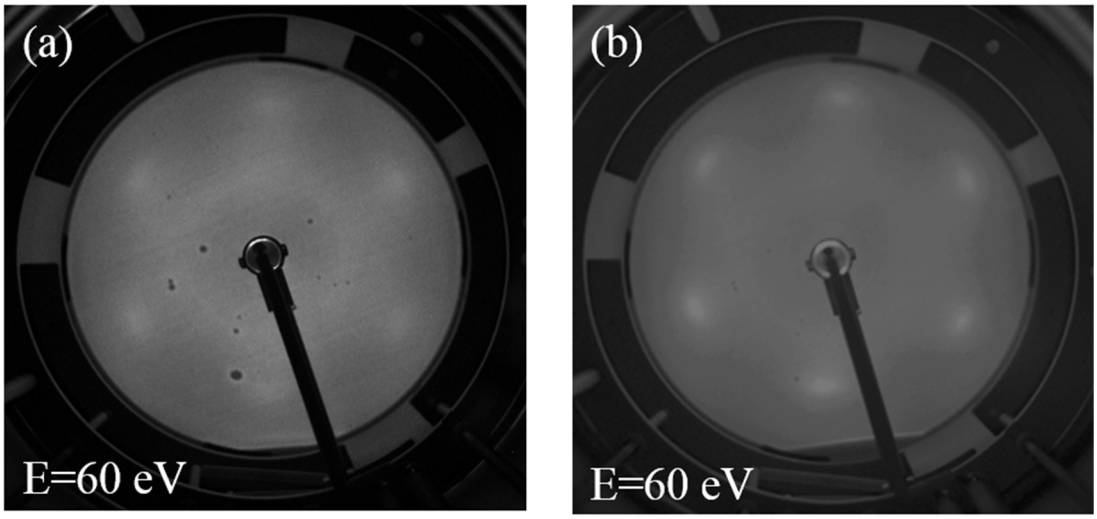

Figure 6 LEED pattern for (a) E2 and (b) E3 sample taken at incident electron energy of 60 eV.

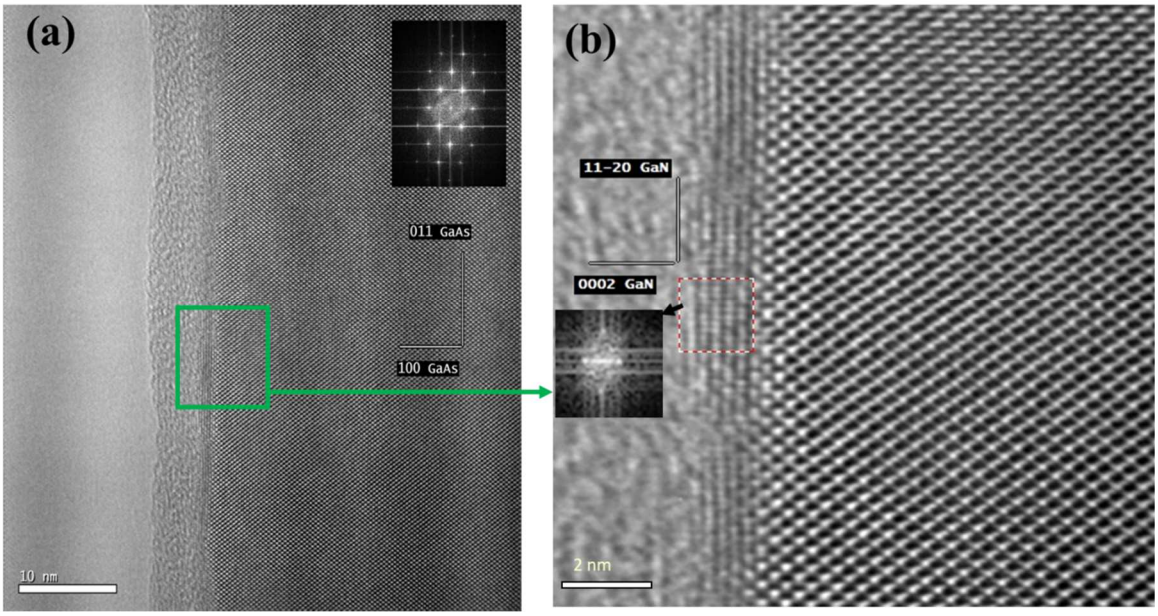

Figure 7 Cross-sectional TEM (a) image of w-GaN on GaAs(100) substrate (E3 sample) (b) higher magnification image showing the w-GaN/GaAs(100) interface.

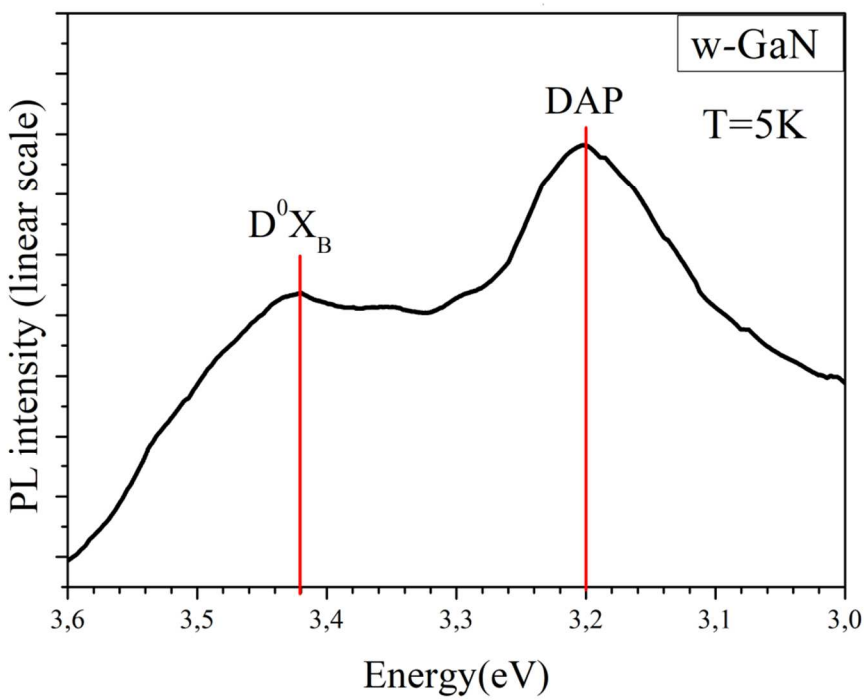

Figure 8 Photoluminescence spectrum for E3 sample recorded at T=5K with a power density of 640 W/cm^2.

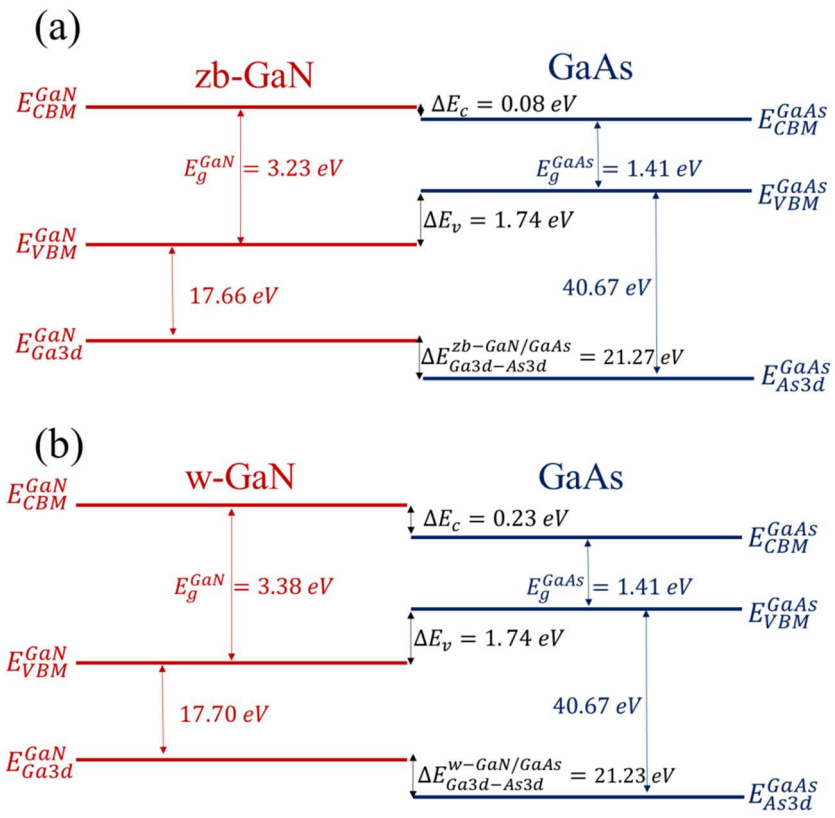

Figure 9 The schematic representation of band alignment at (a) zb-GaN/GaAs and (b) w-GaN/GaAs heterojunctions.